



A new linear plasma device for the study of plasma waves in the electron magnetohydrodynamics regime

GARIMA JOSHI^{1,2,*}, G RAVI^{1,3} and S MUKHERJEE^{1,3}

¹Institute for Plasma Research, Bhat, Gandhinagar 382 428, India

²Nirma University, Sarkhej-Gandhinagar Highway, Chandlodia, Gota, Ahmedabad 382 481, India

³Homi Bhabha National Institute, Anushaktinagar, Mumbai 400 094, India

*Corresponding author. E-mail: jgareema@gmail.com

MS received 22 May 2017; revised 14 November 2017; accepted 28 December 2017;
published online 16 May 2018

Abstract. A new, user-friendly, linear plasma device has been developed in our laboratory where a quiescent ($\Delta n/n \approx 1\%$), low temperature (1–10 eV), pulsed (3–10 ms) plasma can be produced over a large uniform region of 30–40 cm diameter and 40 cm length. Salient features of the device include the flexibility of tuning the plasma density in the range of 10^{10} to 10^{12} cm^{-3} and capability of scanning the plasma and field parameters in two dimensions with a precision of < 1 mm. The plasma is produced by a multifilamentary cathode and external magnetic field by Helmholtz coils, both designed and constructed in-house. The plasma parameters can be measured by Langmuir probes and electromagnetic field parameters by miniature magnetic probes and Rogowski coils. The plasma produced is uniform and essentially unbounded for performing experiments on waves and turbulence. The whole device can be operated single-handedly by undergraduate or graduate students. The device can be opened, serviced, new antennas/probes installed and ready for operation in a matter of hours. Some results on the excitation of electromagnetic structures in the context of electron magnetohydrodynamics (EMHD) are also presented to demonstrate the suitability of the device for carrying out such experiments.

Keywords. Plasma device; plasma characterisation; electron magnetohydrodynamics; whistler wave; plasma source; magnetic coil.

PACS Nos 07.30.-t; 07.30.Cy; 07.55.Ge; 07.87.+v; 07.90.c

1. Introduction

In order to investigate plasma waves and turbulence in a controlled laboratory experiment, it is desirable that the plasma be easily produced in the lab, is uniform, unbounded and has a wide range of density and temperature. It is also desirable that the experimental device is easy to use, right from achieving the desired experimental parameters to obtaining the plasma density and scanning of the experimental space for the plasma and field parameters. Over the years, many devices have been built in different labs around the world, a majority of them linear devices for fundamental studies on plasma waves. It is almost impossible to mention each one of them, let alone describe. We shall only briefly discuss some devices specifically built to study phenomena similar to those occurring in naturally occurring unbounded plasmas. In such devices, the experimental conditions become more stringent because similar physical processes need to be simulated and investigated by

carrying out detailed measurements of plasma and field parameters over a large volume. Also, the plasma parameters need to be modified suitably to accommodate the perturbations in the desired volume.

Some of the earliest devices were small and not suitable for such studies. Plasma produced in these devices were of small volume and had large gradients. There was no control over the instabilities occurring in the main discharge and the discharge volume could not be scanned completely. With the advancement in electronics, new and advanced power sources, storage technology and computers, many difficulties were overcome and later on sufficiently large devices [1] were built that were capable of producing large volume plasmas and sufficiently sophisticated experiments could be performed. Devices were also built which are suitable for studying space plasma, solar physics and fusion-related studies [2]. Other examples include the space physics simulation chamber focussing on ionospheric and magnetospheric phenomena [3], LVPD [4] for investigating

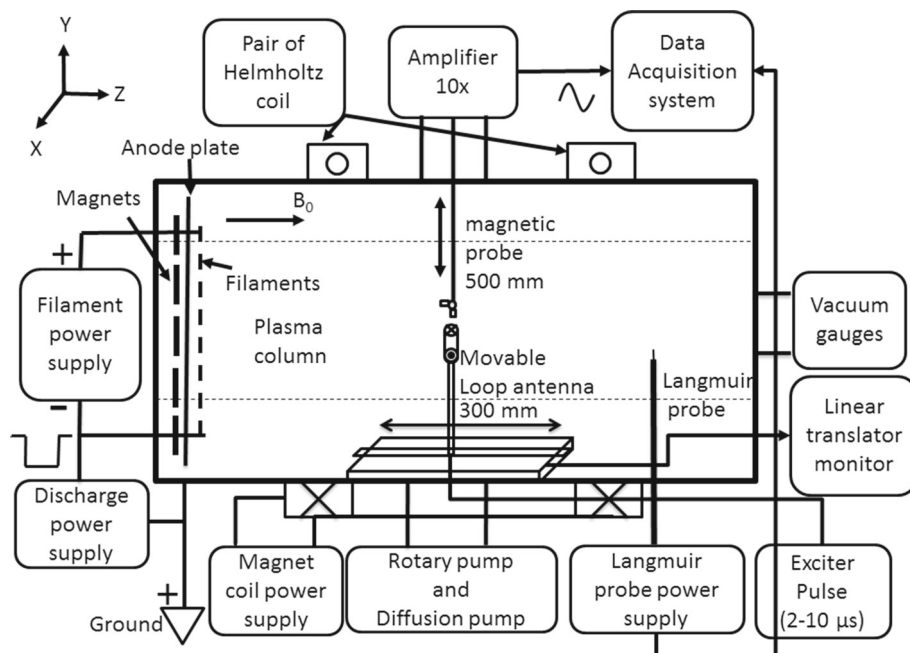


Figure 1. A schematic of the device.

space phenomena, turbulence and transport, a recent one like the Keda Space Plasma Experiment (KSPEX) [5] which has been built to study particle acceleration, transport processes and boundary layer process in ionosphere. A few more devices built recently are the HelCat device [6] for studying turbulence and transport phenomena and KROT device [7] for the simulation of space environment in laboratory. Some of these devices have been built in the recent past. Each device is unique and capable of producing a uniform magnetised plasma with several other features suited for carrying out a particular set of experiments.

In a basic plasma experiment, it is often essential to not just understand the propagation characteristics of the waves but also to investigate the detailed topology. This is because it has been found that many of these waves, especially Alfvén and whistler waves, exhibit force-free characteristics and complex topology [9–12]. Hence, it is imperative that the experimental device is equipped with translators/probe drives that can be used to unravel the two-/three-dimensional spatio-temporal characteristics of the excited structures and is big enough for producing unbounded plasma for the spatial scale lengths in question, yet small enough for ease of handling. This paper presents the construction and development of one such linear plasma device that is sophisticated in its yield but simple enough that it can be single-handedly operated by an undergraduate or graduate student. The device is described in §2, pulsed plasma characteristics are described in §3 and preliminary results from wave experiments are presented in §4. This is followed by summary and discussions in §5.

2. The experimental device

2.1 Vacuum chamber

A cross-sectional schematic of the linear plasma device is shown in figure 1. The device consists of a stainless steel (SS304) single-walled cylindrical vacuum chamber with 2 m length and 1 m diameter. There are two movable hemispherical dish ends, one used for electrical and cooling connection of plasma source and the other for vacuum gauges and vacuum–atmosphere linear translator interface. The other ports on the main chamber are employed for various purposes such as for connecting vacuum pumping system, optical ports, translator arrangement for probes, current injection into antennas, Langmuir probes, gas dosing and so on. The vacuum pumping system enables the attainment of a base vacuum of 3×10^{-6} mbar in the entire system. Detailed internal view and external view of the linear plasma device is shown in figure 2.

2.2 Power supply system

The power supply system consists of several power sources for various purposes. The 100 A \times 32 V filament power supply is a DC regulated power supply used in constant current mode. The DC magnet power supply (60 A \times 30 V) drives the external Helmholtz coil. The plasma discharge is driven by a pulsed power supply of 200 A \times 100 V rating, tunable 3–15 ms flat top and a turn-off time of $\sim 20 \mu\text{s}$ in order to ensure that energetic electrons in the main glow (flat top ON region)

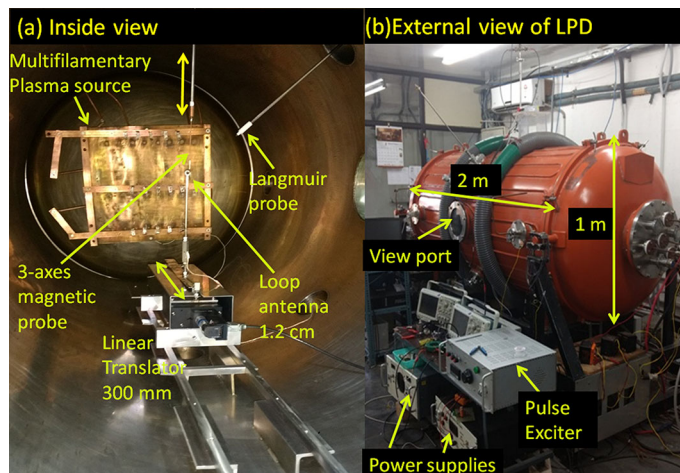


Figure 2. (a) Internal view of linear plasma device and (b) external view of the device.

leave the body of the plasma within a fraction of the time after the voltage is cut off. This renders the plasma quiescent and Maxwellian in the afterglow. Another power supply is used for biasing the Langmuir probe $I-V$ electronics card. The whole filament assembly along with the power supply is biased negative with respect to the chamber that is both positive and grounded.

2.3 Magnet field coils

A simple Helmholtz coil assembly is adopted for the production of uniform magnetic field in the region of interest. The coils are separated by 0.55 m and nearly equal to the radius. Magnetic field figure of merit is ≈ 1 and coils need not be cooled. The field is fairly uniform ($\Delta B/B_0 \ll 0.2\%$) over a large region from the centre of the Helmholtz coils as shown in figures 3a and 3b. It shows the magnetic field profile with variation of z (axial) for different values of r (radial) and variation of r (radial) for different values of z (axial). The magnetic field plotted is the B_z component. In the magnetic coil configuration that we have used, the dominating magnetic field component is the axial component (B_z component) in the region of interest, with the remaining components possessing negligible field value. In figure 3a the curves are shifted to see the magnetic field profile clearly. Also, the profile for different r values in figure 3b is similar. We have mapped the magnetic field in the $y-z$ plane with the help of a Gaussmeter and we found this to be uniform upto 25 cm radially with less than 10% variation in axial and radial directions in the region of interest. Here, magnetic field is plotted from filament source to few distances from the second coil in the axial direction (centre axis) and 2D measurements also show good uniformity.

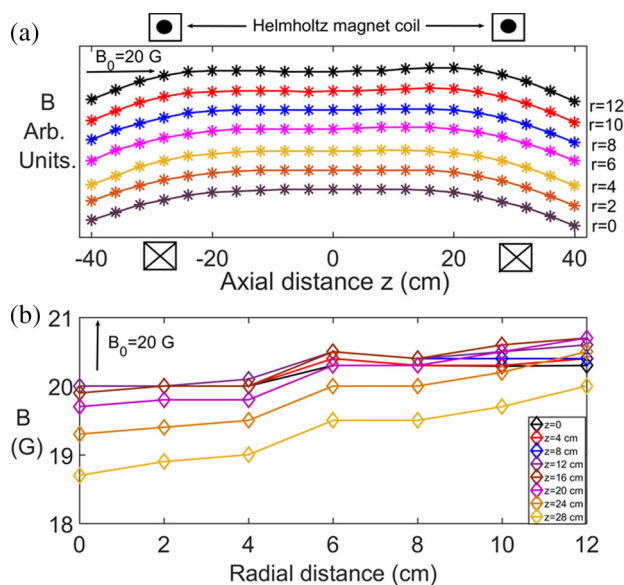


Figure 3. Magnetic field profile is shown in (a) for different radial positions from $r = 0$ (centre position) to $r = 12$ cm and (b) for different axial positions.

2.4 Plasma source

Plasma is produced by a multiflamentary cathode source [8]. It consists of parallel combination of 14 thoriated tungsten filaments. This low-cost source has been designed and fabricated in our laboratory and it consists of copper base plate of $500 \text{ mm} \times 500 \text{ mm} \times 3 \text{ mm}$ dimensions, which is kept in contact with the chamber and acts as anode. Vacuum-compatible permanent magnets (NdFeB) are fixed on the plate in broken line cusp arrangement to make sure that primary electron loss is controlled and are available for plasma production. The electrons emitted from the filaments go towards

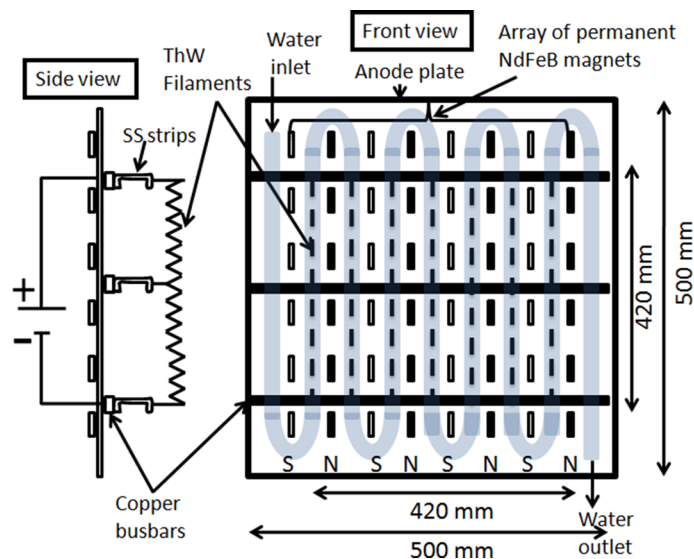


Figure 4. Schematic of the multifilamentary plasma source.

the anode plate, get trapped in the cusp field of the magnets and bounce back towards the chamber. Filaments are triangular and the bending results in more emission of electrons compared to straight wires as has been well established in [13]. The saturation current density can be calculated from Richardson–Dushman’s equation and for the present case it is estimated to be $J \sim 2.8 \text{ A/cm}^2$ for the 0.25 mm diameter thoriated tungsten filaments. To obtain this saturation current density, a temperature of at least 2200 K is required that can be obtained by passing 6–7 A of current through the filaments [13]. The total area of filaments yields a saturation current density of about 50 A. Assuming each primary electron is contributing to the ionisation process, a discharge current of 50 A can easily be obtained. It is shown in later sections that it is indeed so. A schematic of the multifilamentary cathode source is shown in figure 4.

2.5 Diagnostics and data acquisition

Local plasma parameters are obtained using a cylindrical Langmuir probe made of tungsten. A probe array is also used for simultaneous measurement of plasma density and temperature in axial direction as well as in radial direction. As the plasma is pulsed, instead of providing ramp to obtain full I – V curve, ion saturation current is collected by keeping the bias voltage fixed across the load resistor and then changing it from -100 V to $+20 \text{ V}$. The probe current is collected at the probe tip through an I – V electronics card and output is measured using the oscilloscope. An analysis of the data yields density and temperature.

For detecting perturbed wave magnetic fields, magnetic pick-up coils (probes) are used, the design of which becomes critical in the event of detecting small-amplitude high-frequency wave fields. A magnetic probe should have good sensitivity, i.e., high signal to noise ratio and excellent frequency response so that it can measure rapid fluctuations of magnetic field and also minimal perturbing effect on the plasma. For experiments specific to the EMHD regime, we need to measure time-varying magnetic field associated with electromagnetic waves of dimensions $\sim \text{skin depth} \geq 1 \text{ cm}$. Therefore, the magnetic probe used is miniature with minimal perturbing effect on the plasma. But this leads to a compromise over the sensitivity of the probe. Secondly, it is almost impossible to provide an electrostatic shield in the form of a metallic cover with a cut, both because of the small size of the probe as well as decreasing sensitivity due to the formation of eddy currents. The magnetic probe used in the experiments in this work is a miniature, bifilar 3-axes probe. A photograph of the magnetic probe is shown in figure 5. Each probe is orthogonal to the other two so that all the three magnetic field components B_x , B_y and B_z can be measured simultaneously. The probe design is similar to the one quoted in an earlier work [14,15] and also has been used in others [4]. This design has certain advantages over the regular centre-tapped design in the sense that only two connections need to be taken out, unlike three in the centre-tapped design. Thus, it does not require the use of a subtraction transformer or a differential amplifier before acquisition. For other experiments, appropriate probes can always be designed, developed and installed.

The diagnostics also include a Rogowski coil for the measurement of current associated with the plasma

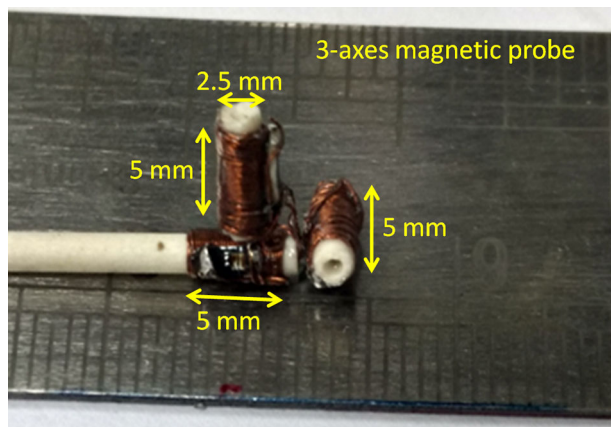


Figure 5. 3-Axes magnetic probe used in our experiments.

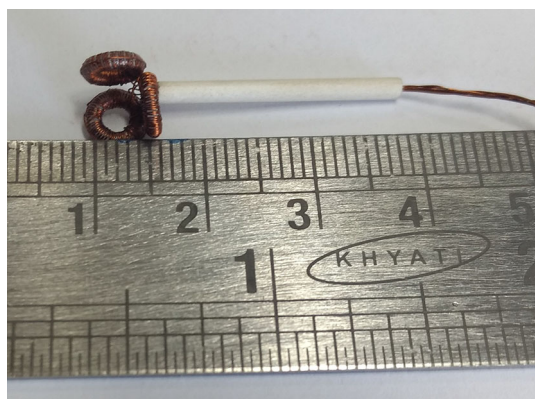


Figure 6. 3-Axes Rogowski coil for the measurement of current associated with the launched electromagnetic waves.

waves. The coil is essentially a toroidal solenoid that encircles a current flowing through a conductor. The coil used in our experiments is wound using thin vacuum-compatible wires on a rectangular cross-sectional ceramic core. As it is air-cored, it exhibits good linearity and also is non-intrusive, i.e. the coil does not load the circuit carrying the current to be measured under certain conditions of impedance matching. Figure 6 shows a photograph of the coil used in our experiments that can measure high frequencies ranging from 100 kHz to 10 MHz and the current to be measured is related to the voltage induced by a proportionality constant.

Two digital storage oscilloscopes are used for acquiring the data. One is used for acquiring plasma parameters such as discharge voltage, current, floating potential and Langmuir probe characteristics and the other is for antenna current pulse and transient magnetic fields. The data are saved in USB drives and then used for data analysis.

3. Pulsed plasma characteristics

Argon plasma is produced by applying discharge voltage pulse to the heater (thoriated tungsten filaments) of the cathode source at $\sim(2-5) \times 10^{-4}$ mbar pressure. This pressure range is ideally suited for such experiments as the plasma is rendered collisionless for the time scale of the explored phenomena. Discharge voltage pulse consists of 3–15 ms negative biased pulses with ON/OFF time of $\sim 10-20 \mu\text{s}$ with almost flat top region for the selected duration. The properties of pulsed plasma are obtained by conventional method using Langmuir probes at different axial and radial positions inside the chamber. In order to obtain a suitable density, filament current is varied first and fixed for maximum emission current density values. This is achieved by changing filament current and raising the temperature of the filaments up to 2200 K, at which filaments become copious emitters of electrons [16].

For every discharge voltage pulse of a few ms duration, a glow discharge pulsed plasma is formed. The flat region of the discharge voltage pulse signifies the main glow region; the afterglow region starts as soon as the voltage is cut off. The current transformer gives information about the plasma discharge current and a Langmuir probe picks up the floating potential information. Figure 7 shows pulsed waveforms of discharge voltage V_d , discharge current I_d and floating potential V_f . In order to estimate plasma parameters, the bias on this probe is changed from -100 to 20 V in steps of 1 V (and sometimes in smaller steps near the floating potential region) and repeatable pulsed plasma shots are taken. Averaging of four shots has been taken and acquired in the oscilloscope. After obtaining this information, complete $I-V$ characteristics are constructed at each instant of time in the main discharge time and after that. In figure 8, current voltage characteristics are plotted at one point of time in the main glow region and at $150 \mu\text{s}$ in the afterglow region. The temperature is estimated using the exponential part of the $I-V$ curve assuming Maxwellian electrons. In the main glow region the temperature obtained varies from 7 to 10 eV and in the afterglow region from 2 to 4 eV. The reason behind the fall in temperature from the main glow to afterglow is that in the main glow region electrons with a broad energy distribution from filaments are continuously participating in the formation of plasma. However, when the pulse is switched off, highly energetic electrons are lost to the walls quickly due to their mobility and the bulk plasma remains with lower energy electrons that diffuse slowly. Thus, the temperature falls and reduces to 1 eV at $250-300 \mu\text{s}$ in the afterglow region. The main glow is filled with bulk plasma electrons as well as energetic

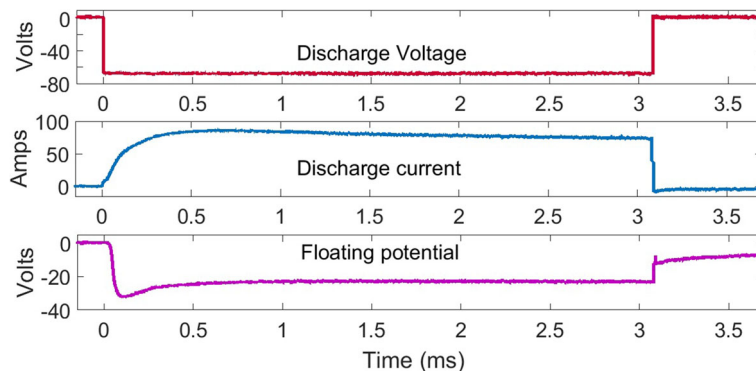


Figure 7. Typical discharge voltage, discharge current and floating potential.

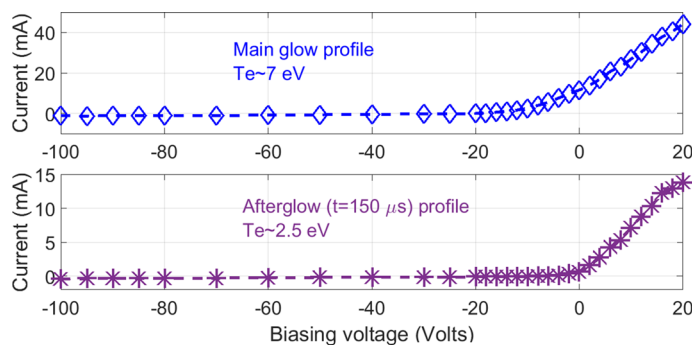


Figure 8. Langmuir probe $I-V$ characteristics extracted from the pulsed $I_{i,sat}$ for each probe voltage: mainglow and afterglow.

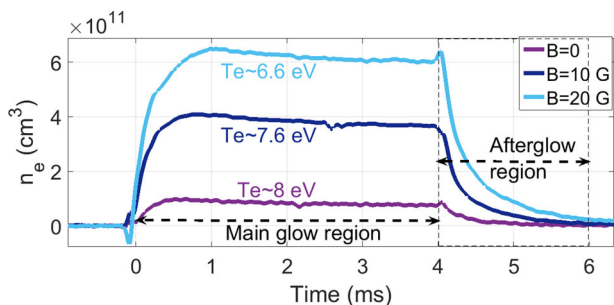


Figure 9. Plasma density for $B = 0$, $B = 10$ G and $B = 20$ G in the main glow region.

electrons and these highly energetic electrons also contribute to the overall temperature in addition to a tail component in the Maxwellian. The afterglow, on the other hand is current free ($V_d = 0$) compared to the main glow, which consists of only purely Maxwellian electrons without any tail components; therefore also quiescent and uniform. The -20 V shift in the floating potential is obtained by a single Langmuir probe. Discharge is struck for different background external magnetic fields. Figure 9 shows the pulsed density profile for $B = 0, 10$ and 20 G. When magnetic field

is applied, loss of electrons to the wall reduces and this results in increase in the plasma density at a given time. With increasing magnetic field, the density decays more slowly in the afterglow. The temperature also changes with magnetic field. Temperature is lowered with increase in the externally applied background magnetic field as can be seen from the figure. Distinct regions in the figure correspond to the main glow in the 0–4 ms duration and afterglow in the 4–6 ms duration. The external magnetic field is DC and always ON even when the voltage is cut off. For clarity, this afterglow region is zoomed in figure 10 for $B = 0, 10$ and 20 G. Temperature values are shown for a particular instant of time ($150 \mu s$) in the afterglow for different values of magnetic field. It is seen that temperature changes only marginally as the external magnetic field is increased, which could be within the experimental errors and cannot be elaborated. Although the decay in density is slowed down with increasing magnetic field, the trend is different for different values of the field. As a single Langmuir probe provides only local plasma information, a multiarray Langmuir probe is used that can span a region of 60 cm axially and can be moved radially as well.

Figure 11a shows axial plasma density profile for the main glow region and figure 11b shows the axial plasma

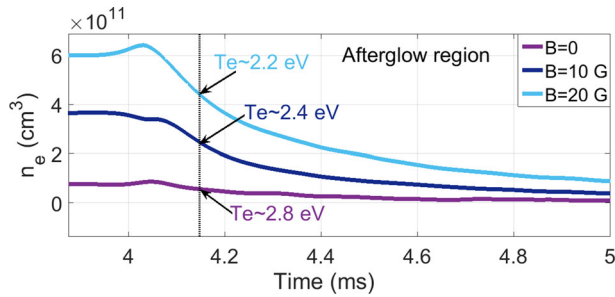


Figure 10. Plasma density for $B = 0$, $B = 10$ G and $B = 20$ G.

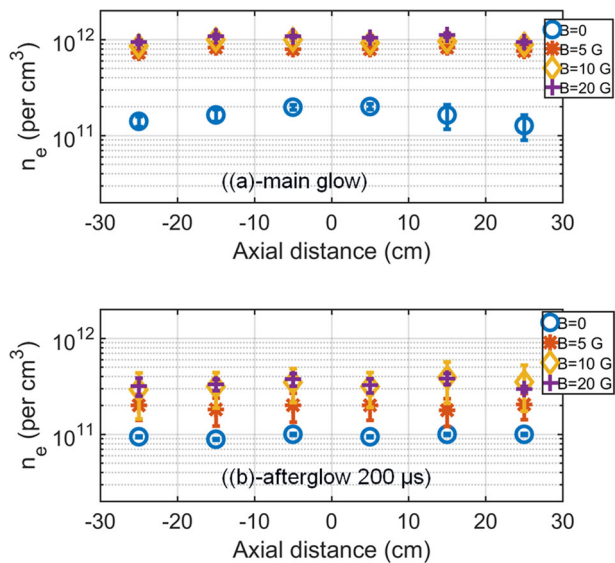


Figure 11. Axial plasma density profile for (a) main glow region and (b) afterglow region.

density profile at $200 \mu\text{s}$ in the afterglow region. It is evident that change in axial plasma density is marginal beyond an externally applied magnetic field of 10 G. The peak magnetic field value is $\sim 10^{12} \text{ cm}^{-3}$ in the main glow and then reduces to an order lesser in afterglow. The axial uniformity of plasma in the 60 cm region is calculated to be $\Delta n/n \sim 15\%$ and hence can be considered as a more or less uniform plasma region. While there is one order change in density between the magnetised and unmagnetised plasma cases, there is very little change in the density between $B = 10$ G and $B = 20$ G cases. The reason for the marginal change is that on increasing the magnetic field, there is a confinement of slightly more highly energetic electrons which were not confined in the earlier case ($B = 10$ G). As the number of neutrals available for ionisation is fixed, the value does not increase much.

Figure 12a shows the variation of plasma density as a function of radial distance for different magnetic

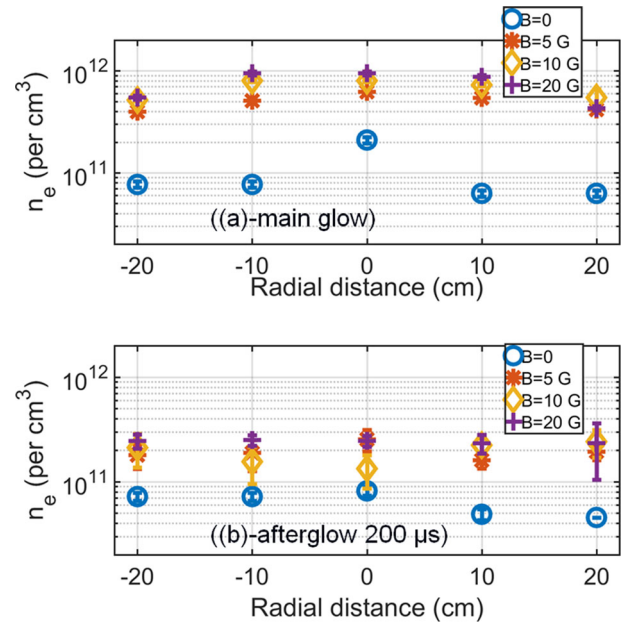


Figure 12. Radial plasma density profile for (a) main glow region and (b) afterglow region.

fields in the main glow region. For $B = 0$, maximum density obtained is $\sim 2 \times 10^{11} \text{ cm}^{-3}$ in the central region and decreases to $6 \times 10^{10} \text{ cm}^{-3}$ towards the chamber wall. The density is maximum at the centre while there is a sharp gradient towards the chamber wall. For $B = 10$ G, the maximum density reaches $8 \times 10^{11} \text{ cm}^{-3}$ and reduces to $5.4 \times 10^{11} \text{ cm}^{-3}$ near the edge and seems to be more uniform than when $B = 0$. For $B = 20$ G, maximum density reaches $1 \times 10^{12} \text{ cm}^{-3}$ and reduces to $5.2 \times 10^{11} \text{ cm}^{-3}$ near the edge which is quite uniform and well suited for wave studies in a uniform and unbounded plasma. However, at increased magnetic field, the density is flatter and yields a more uniform spatial region. The sudden increase in the plasma density from unmagnetised, i.e., $B = 0$ to $B = 10$ G magnetised plasma is due to the confinement of primary electrons, as the mean free path of electron neutral argon atom collision in the absence of magnetic field is approximately a few metres whereas it is about 2 cm for $B = 10$ G and 1 cm for $B = 20$ G. Figure 12b shows plasma density as a function of radial distance in the afterglow region at $200 \mu\text{s}$ after the discharge voltage is switched off, again for different values of external magnetic field. The afterglow plasma density values are lower than their main glow density values. In an unmagnetised plasma, the calculated mean free path is $\lambda_{\text{mfp}} \sim 1$ m and diffusion coefficient is $D_{\text{unmag}} = (\pi/8)\lambda^2 v_m \text{ m}^2/\text{s} \sim 3.35 \times 10^4 \text{ m}^2/\text{s}$. In a magnetised plasma, gyroradius $r_{Le} \sim 4$ mm for $B = 10$ G and $D_{\text{mag}} = (\pi/8)r_{Le}^2 v_m \text{ m}^2/\text{s} \sim 1.5 \text{ m}^2/\text{s}$. It is obvious that loss of plasma to the wall decreases

in the case of magnetised plasma and thus plasma density increases [18]. As the source is ON during the main glow, the plasma density has a peaked profile with a decaying profile radially outwards. On the other hand, when the voltage is cut off, the highly energetic electrons from the source no longer play any role and the bulk plasma just decays and lost to the wall. In this process, the peaked profile gives way to a more flatter one because the supply of electrons is cut off. Thus, a more uniform radial density profile can be obtained in the afterglow region. Specific profiles can be obtained if one goes further at larger times in the afterglow where profiles can be flatter but peak density may be lower and not suitable for our experiments.

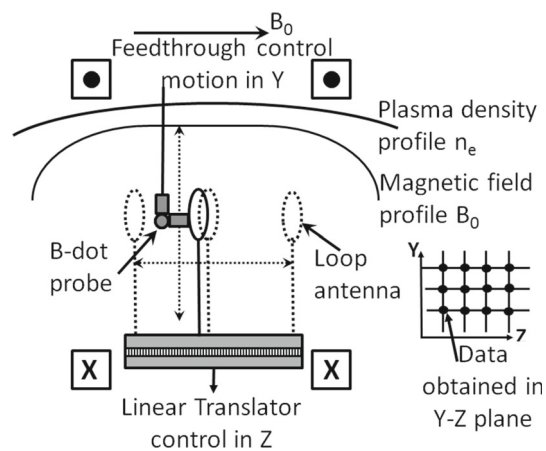


Figure 13. Schematic of 2D measurement.

4. Wave excitation experiments

Optimisation of pulsed plasma parameters is very important and necessary to find the suitability of carrying out the intended experiments on waves in the context of EMHD [17]. This involves a critical analysis of the plasma parameters' spatiotemporal context, both in space and time. Our experimental results in the previous section indicate that it is possible to achieve these conditions in this device. In order to demonstrate the suitability of the device to support electromagnetic waves in the EMHD regime, experiments are carried out in the plasma of density $n_e \sim 1 \times 10^{11} \text{ cm}^{-3}$ and $T_e \sim 2\text{--}4 \text{ eV}$. A short-duration current pulse is fed into a single-turn 1.2 cm diameter loop antenna that is made of semirigid 50 Ω coaxial cable but insulated from the plasma. The pulse has rise and fall times of $\sim 200 \text{ ns}$ and flat top of $\sim 10 \mu\text{s}$ and is fed into the antenna at approximately 150 μs in the afterglow plasma, i.e. after the discharge voltage is cut off. This is the time when plasma density is reasonably uniform and suitable for excitation of electromagnetic waves in the EMHD regime (see §3). The plasma temperature also drops down to $\sim 2\text{--}3 \text{ eV}$ from 9 eV in the main glow.

For exciting the perturbations, the exciter pulse is synchronised with discharge voltage pulse in such a way that it always occurs at a fixed point of time in the afterglow plasma. The plasma responds to the loop antenna pulse by exciting one whistler wave during the rise of the pulse and another during the fall. During the flat top no wave is excited. As the current is small ($\sim 1 \text{ A}$, $\Delta B/B_0 \ll 1$), the waves are linear in nature. The wave magnetic field is detected using a three-axes magnetic probe assembly, each probe with diameter 2 mm, length 3 mm and 30 turns. Data are acquired both in the presence and absence of plasma and the difference yields the wave magnetic field.

Many complex probe drives have been used in earlier work [2] that help probes to scan the full three-dimensional plasma volume while the exciter/antenna is fixed at a given position. Highly repeatable plasma shots are employed to obtain wave propagation and topological characteristics. For our experiment, a novel scheme is employed. Instead of mounting the probe on the drive and scanning the plasma volume, we have used two separate drives to move both the antenna and probes independently in the spatial regime where density has been found to be uniform. A low-speed, high-precision linear translator is fixed inside the chamber in the region of uniform magnetic field and plasma density. A schematic of the arrangement is shown in figure 13. The antenna can be moved in a direction parallel to the magnetic field and device axis up to 300 mm in reverse and forward directions with a precision of 1 μm . A 3-axes magnetic probe is mounted on the top port for radial movement. The motion of the probe is controlled by a stepper motor with 3–4 mm precision. The functioning of the stepper is decided by the motor driver which is controlled by a microcontroller purchased locally. A software for the desired motion is fed into the microcontroller. A small electronic switch is also built in our lab for upward and downward motions and in steps. In order to perform wave experiments in afterglow plasma, the density should be uniform over the time when the antenna excitation and wave detection is on, which may span over a few microseconds at the maximum. To make sure that this condition is met every time, a feedback from pulsed power supply is fed into the exciter when the discharge voltage is cut off. At this moment, a time delay is introduced and exciter pulse is given. Thus, formation of plasma and exciter pulse are synchronised appropriately. The translator is vacuum compatible and can be moved by controls provided by a computer software. Using this technique, we have obtained the 2D topology

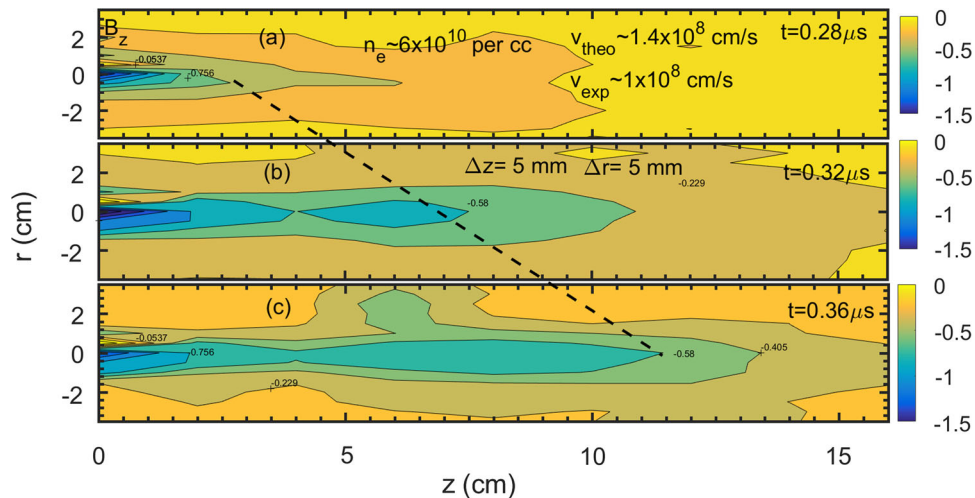


Figure 14. Contour plot showing B_z component represents spatiotemporal plot (a) at $t = 0.28 \mu\text{s}$, (b) at $t = 0.32 \mu\text{s}$ and (c) at $t = 0.36 \mu\text{s}$.

of the excited structures using highly repeatable plasma shots. For obtaining this, the antenna is initially placed at the edge of the region and after the first shot, the magnetic probe is moved vertically and plasma shots are repeated. Thus, radial data are obtained for one z position. After this, the antenna is moved and fixed at another axial location and the magnetic probe is moved again in the vertical direction. A contour plot of the $B_{z,\text{wave}}$ component is shown in figure 14.

The probe is moved in steps of 5 mm in radial direction and antenna in steps of 20 mm in axial direction, although the encoder resolution of the translator is as good as $1 \mu\text{m}$.

The theoretical dispersion relation of the whistler wave is

$$\omega = \frac{kk_z\omega_{pe}}{k^2 + \omega^2/c^2} \left[1 - i \frac{kv_e}{k_z\omega_{pe}} \right], \quad (1)$$

where $k = \sqrt{k_\perp^2 + k_z^2}$, $k_z = k_\parallel$. Under the EMHD approximation $L_e \ll L \ll L_i$ and $\omega_{ci} \ll \omega \ll \omega_{ce} \ll \omega_{pe}$, where L and ω are spatial and temporal scale lengths of the perturbations, L_e and L_i are the electron and ion Larmor radii respectively, ω_{ci} and ω_{ce} are ion gyrofrequency and electron gyrofrequency respectively, $\omega = 2\pi f$ is the perturbation frequency, ω_{pe} is the plasma frequency. For collisionless and quasiparallel propagation, the above expression reduces to $\omega/k = \omega/k_\parallel = c/\omega_{pe}\sqrt{\omega_{ce}}$. The value of k is not calculated but it is subsumed in ω/k_\parallel . The propagation speed of the wave is then calculated as $v_{\text{theory}} = 1.4 \times 10^8 \text{ cm/s}$ and it is nearly equal to the experimentally calculated value $v_{\text{exp}} = 1 \times 10^8 \text{ cm/s}$. Speed of wave propagation is high due to low density of plasma. Dashed line shows the

evolution of the wave front in space and time. It is clear that perpendicular extent of the wave is nearly 4 cm which is approximately twice the diameter of the loop antenna, while the axial extent of the wave is several times the perpendicular extent. This analysis can be repeated for all the three components of the magnetic field from which information about the wave currents and time-varying electric fields associated with the electromagnetic structures can be extracted. More experiments, along with those in the nonlinear regime where $B_{\text{wave}} \geq B_0$ and in a regime where $k_{de} \geq 1$, are underway and results will be published elsewhere soon.

5. Summary and discussion

A new linear device has been developed which is capable of producing a sufficiently large, uniform, moderately high-density, low-temperature plasma for carrying out basic plasma experiments. The plasma parameters can be tuned by changing the filament current, magnetic field, density uniformity etc., in order to perform experiments on a wide range of experimental parameters. For example, the density can be tuned over the range 10^{10} – 10^{12} cm^{-3} at different external magnetic field values by either adjusting the discharge voltage or the filament current. In fact, plasma densities of $\sim 10^{11} \text{ cm}^{-3}$ can be obtained even at zero external magnetic field. In the particular context of performing experiments in the EMHD regime where the characteristic perpendicular wavelengths are of the order of 1–5 cm, it is required that the plasma region be sufficiently large and uniform to accommodate several of these perturbations. We find that the device satisfies these conditions with plasma of

Table 1. The parameters which satisfy the EMHD condition.

Plasma parameter	Values
Electron gyrofrequency, ω_{ce}	8.80×10^7 rad/s
Electron plasma frequency, ω_{pe}	1.78×10^{10} – 3.9×10^{10} rad/s
Electron gyroradius, r_e	3–8 mm
Electron inertial length, d_e	0.5–3 cm
Ion gyrofrequency, ω_{ci}	1.20×10^3 rad/s
Ion plasma frequency, ω_{pi}	1.04×10^7 rad/s
Ion gyroradius, r_i	40 cm
Ion inertial length, d_i	5.76×10^2 cm
Wavelength, λ	15–30 cm
Debye length ($T_e = 1$ eV)	~ 0.03 mm

40 cm (radial) and 60 cm (axial) dimensions. The basic wave parameters are calculated and shown in table 1. These parameters are obtained experimentally and satisfy the spatial and temporal range for performing the studies intended on EMHD and related phenomena.

The device opens up possibilities of performing several interesting and unique plasma experiments for the exploration of various phenomena, e.g. it gives us the flexibility of (i) switching from electromagnetic to hydrodynamic regime of EMHD plasma and (ii) flexibility of working in either $kd_e \ll 1$ or $kd_e \geq 1$ regimes. By using appropriate antennas with sufficient turns, it also gives the flexibility to work either in linear or non-linear regimes. The afterglow at $B = 0$ also offers a unique regime where density of 10^{10} cm^{-3} is available in the afterglow. This regime is particularly useful to conduct experiments on electron vortices and their interaction among themselves. The region within 150–200 μs in the afterglow offers right conditions for the chosen wave plasma experiments. Detailed results on the excitation of EMHD structures are already reported elsewhere [19].

References

- [1] R L Stenzel, *Phys. Fluids* **19**, 857 (1976)
- [2] W Gekelman, H Pfister, Z Lucky, J Bamber, D Leneman and J Maggs, *Rev. Sci. Instrum.* **62**, 2875 (1991)
- [3] W E Amatucci, D N Walker, G Ganguli, D Duncan, J A Antoniadis and J H Bowles, *J. Geophys. Res.* **103**, 11711 (1998)
- [4] S K Mattoo, V P Anitha, L M Awasthi, G Ravi and LVPD Team, *Rev. Sci. Instrum.* **72**, 3864 (2001)
- [5] Yu Liu, Zhongkai Zhang, Jiuhou Lei, Jinxiang Cao, Pengcheng Yu, Xiao Zhang, Liang Xu and Yaodong Zhao, *Rev. Sci. Instrum.* **87**, 093504 (2016)
- [6] Alan G Lynn, Mark Gilmore, Christopher Watts, Janis Herrea, Ralph Kelly, Steve Will, Shuangwei Xie, Lincan Yan and Yue Zhang, *Rev. Sci. Instrum.* **80**, 103501 (2009)
- [7] Mikhail E Gushchin, Sergey V Korobkov, Alexander V Kostrov, Askold V Strikovskiy, Vladimir I Gundorin, Alexander G Galka and Dmitry A Odzerikho, *Proceedings of the 18th Topical Conference on Radio Frequency Power in Plasmas* (Gent, Belgium, 2009) pp. 659–666
- [8] L M Awasthi, G Ravi, V P Anitha, P K Srivastava and S K Mattoo, *Plasma Sources Sci. Technol.* **12**, 158 (2003)
- [9] R L Stenzel, J M Urrutia and C L Rousculp, *Phys. Fluids B* **5**, 325 (1993)
- [10] J M Urrutia, R L Stenzel and C L Rousculp, *Phys. Plasmas* **1**, 1432 (1994)
- [11] R L Stenzel, J M Urrutia and C L Rousculp, *Phys. Plasmas* **2**, 1114 (1995)
- [12] C L Rousculp, R L Stenzel and J M Urrutia, *Phys. Plasmas* **2**, 4083 (1995)
- [13] K N Leung, T K Samec and A Lamm, *Phys. Lett. A* **51**, 490 (1975)
- [14] Peter Beiersdorfer and Eugene J Clothiaux, *Am. J. Phys.* **51**, 1031 (1983)
- [15] P K Loewenhardt, B D Blackwell and Beichao Zhang, *Rev. Sci. Instrum.* **64**, 3334 (1993)
- [16] K W Ehlers and K N Leung, *Rev. Sci. Instrum.* **50**, 356 (1979)
- [17] S Kingsep, K V Chukbar and V V Yankov, in: *Reviews of plasma physics* edited by M A Leontovich (Consultants Bureau, New York, 1990) Vol. 16, p. 243
- [18] Michael A Lieberman and Alan J Lichtenberg, *Principles of plasma discharges and materials processing*, 2nd edn (John Wiley & Sons Inc, Hoboken, New Jersey, 2005).
- [19] Garima Joshi, G Ravi and S Mukherjee, *Phys. Plasmas* **24**, 122110 (2017)